PCCP

Accepted Manuscript

ROYAL SOCIETY OF CHEMISTRY

Journal Name

ARTICLE

In situ growth of TiO_2 nanocrystals on g-C_3N_4 for enhanced photocatalytic performance

Hong Li[b], Liang Zhou[a], Lingzhi Wang[b], Yongdi Liu[a], Juying Lei[a,*], Jinlong Zhang[b,*]

Well dispersed TiO_2 nanocrystals with (001) facets were successfully grown in-situ on g-C_3N_4 through a facial solvothermal method. The resultant TiO_2/g-C_3N_4 composites exhibit remarkably higher efficiency for photocatalytic degradation of phenol as compared to pure catalysts (g-C_3N_4 or TiO_2) or mechanically mixed TiO_2/g-C_3N_4. The optimal composite with 11.2wt% TiO_2 showed the highest degradation rate constant, which is 2.8 times that of pure g-C_3N_4, 2.2 times that of pure TiO_2, and 1.4 times that of the mechanically mixed TiO_2/g-C_3N_4 respectively. The enhanced photocatalytic activity is mainly attributed to the effective charge separation derived from two aspects: (1) well matched energy level between the TiO_2 and g-C_3N_4; and (2) the uniform and close contact between the TiO_2 and g-C_3N_4 resulted from the in situ growth of highly dispersed TiO_2 nanocrystals. The TiO_2/g-C_3N_4 hybrid material prepared in this study is expected to provide a good foundation for the further design and synthesis of advanced TiO_2/g-C_3N_4-based functional materials and the in situ growth method developed is hopeful to provide a new strategy for the synthesis of other semiconductor-modified g-C_3N_4 materials.

Introduction

Semiconductor-based photocatalysis has been considered to be one of the most promising and attractive techniques in terms of solar energy conversion and treatment of organic pollutants[1,2]. In the past decades, various semiconductor materials such as metal oxides[3-5], sulfides[6,7], and oxynitride[8,9] have been developed as photocatalysts under UV or visible light irradiation. Very recently, a polymeric semiconductor, graphite-like carbon nitride (g-C_3N_4)[10], has been reported as a metal-free and sustainable photocatalyst[11,12], which exhibits high photocatalytic performance for hydrogen production from water splitting. The catalytic performance of g-C_3N_4 for the photodegradation of organic pollutants in waste water was also investigated[13,14]. However, the relatively low quantum efficiency of pure g-C_3N_4 still limits its practical application due to the fast recombination of photo-generated charge carriers[15,16]. To resolve this problem, one of the efficient strategies is coupling g-C_3N_4 with other semiconductors to form heterojunction structures. Various semiconductors, such as, ZnO[17], TiO_2[18-21], $TaON$[22], $ZnWO_4$[23], $BiPO_4$[24] and Bi_2WO_6, have been coupled with g-C_3N_4 to increase the separation efficiency of photo-generated electron-hole pairs, thus to promote the photocatalytic activity.

Among the many kinds of semiconductors mentioned above, TiO_2 has been regarded as one of the most attractive candidates due to its non-toxicity, good stability, high activity and its appropriate band position which can well matched with that of g-C_3N_4 to promote efficient separation of photo-generated charge carriers[25-28]. Therefore, great efforts have been made to prepare and study TiO_2/g-C_3N_4 composited photocatalysts. For example, Zhu et al[18] prepared TiO_2/g-C_3N_4 composite with evident performance enhancement by ball milling of TiO_2 and g-C_3N_4. Fu et al[29] reported a solid-state approach to synthesizing g-C_3N_4 coated TiO_2 nanocomposites from urea and commercial TiO_2 precursors. Park et al developed novel visible light active graphitic carbon nitride TiO_2 composite through a thermal transformation methodology. In view of the previous studies, there are mainly three strategies for the preparation of the TiO_2/g-C_3N_4 composite: (1) mixing the pre-synthesized TiO_2 and g-C_3N_4 by means of heating, grinding or ball milling[30-33]; (2) calcinating commercial available TiO_2 or pre-synthesized TiO_2 with precursors of g-C_3N4[34-36]; (3) in situ growth of TiO_2 on pre-synthesized g-C_3N_4[30,37-39]. The first method by using physical mixing is easy to operate and beneficial for scale up, however, uniform mixing and close contact between the two components may not be quite easy to achieve. The second method allows for selection or structure design of the TiO_2 for use, but the high temperature calcinations is prone to resulting in aggregation of TiO_2, which may bring negative impact on the improvement of photocatalytic activity. The third method by in situ growth of TiO_2 doesn't have the mentioned drawbacks of the former two methods, however, because of the rapid hydrolysis of titanium precursor, it's

[a.] *State Environmental Protection Key Laboratory of Environmental Risk Assessment and Control on Chemical Process, East China University of Science and Technology, 130 Meilong Road, Shanghai 200237, P. R. China. Email: leijuying@ecust.edu.cn.*
[b.] *Key Lab for Advanced Materials and Institute of Fine Chemicals, East China University of Science and Technology, 130 Meilong Road, Shanghai 200237, P. R. China. Email: jlzhang@ecust.edu.cn*

difficult to achieve ultradispersed TiO_2 nanocrystals on the surface of g-C_3N_4[40] and controlling the microstructures of coupled TiO_2 with desired dispersity and size distribution is still a great challenge[41].

Herein, we developed a facial solvothermal method for the in situ growth of TiO_2 nanocrystals on g-C_3N_4. It is remarkable to find that TiO_2 nanocrystals with small particle size (<20 nm) are highly dispersed on the surface of the g-C_3N_4. In addition, exposed high energy (001) facet of TiO_2 nanocrystals was found, which has been widely evidenced by theoretical and experimental researches to be more reactive than the thermodynamically stable (101) facets due to their higher surface energy[42]. The resultant TiO_2/g-C_3N_4 composites exhibit considerable higher efficiency for photocatalytic degradation of phenol as compared to pristine catalysts (g-C_3N_4 or TiO_2) or mechanically mixed TiO_2/g-C_3N_4. The mechanism for the enhanced photocatalytic performance has also been discussed. The TiO_2/g-C_3N_4 hybrid material prepared by this facial solvothermal method is expected to provide a good foundation for the further design and synthesis of advanced TiO_2/g-C_3N_4-based functional materials.

Experimental details

Synthesis of g-C_3N_4

g-C_3N_4 was synthesized by heating melamine powder. 6 g of melamine powder was put into an covered alumina crucible and heated in a muffle furnace. At first, the powder was heated to 500℃ at a speed of 2℃ min^{-1} and kept in this temperature for 2 h, then heated to 520 ℃ in 10 min and keep 2 h. After cooling to room temperature, the light yellow g-C_3N_4 was obtained. The product was grounded into powder for further usage.

Preparation of TiO_2/g-C_3N_4

1.5 mL of TBOT was added into 20 mL of ethanol under vigorous agitation. After stirring for 15 min, little yellow transparent solution was obtained. This solution was labeled as A. During the procedure, pay attention to moisture to prevent hydrolysis of titanium source. At the same time, 0.5 g of ammonium acetate (AMAT) was dissolved into 15 mL of ethanol followed by 15 min vigorous stirring. After that, a certain amount of g-C_3N_4 was added into this solution. The suspension was labeled as B. The two solutions of A and B were mixed at room temperature and shifted into 100 mL of Teflon reaction kettle. Then 30 mL of anhydrous ethanol was added to make the total volume became 65 mL and the filling rate reached about 65%. After screwing and sealing the stainless steel outer sleeve well, the Teflon reaction kettle was kept in a 180 ℃ electric thermostatic blast dryer for 18 h and then cooled to room temperature. The suspension was centrifuged for 15 min at a speed of 4000 r min^{-1}, followed by multiple ultrasonic washing with ethanol, Then the sample was dried in 60 ℃ vacuum oven overnight. The samples were labeled as TiO_2/g-C_3N_4(m), where m represented the quality of g-C_3N_4 added in the preparation process. Furthermore, we also prepared compared sample, and the specific process is as follow: 0.8 g g-C_3N_4 was mechanically grinded with 0.1 g TiO_2 nanocrystalline, then was labelled g-C_3N_4+TiO_2(8:1).

Photocatalytic activity test

The photocatalytic activity of the samples was tested by degradation of phenol at room temperature using a 300W Xe lamp with AM 1.5 filter to simulate solar light source. 0.04 g catalyst powder was put into 40 mL of 10 mg/L^{-1} phenol aqueous solution. And it's worth noting that the concentration are the same for all investigated catalysts. At first, the system was stirred in darkness for 30 min to make the catalyst dispersed in phenol solution and reach the adsorption-desorption equilibrium. After 30 min dark reaction, 2 mL of solution was taken out to determine the adsorption ability of every sample. Then light irradiation was turn on, after which 2 mL of solution were taken out per 30 min. All the solution samples obtained were centrifuged at the speed of 1200 r min^{-1} for 10 min, then the concentration of phenol was tested by HPLC.

Results and discussions

The TiO_2 nanocrystals were grown onto g-C_3N_4 by a solvothermal treatment of TBOT and g-C_3N_4 in ethanol in the presence of AMAT at 180 ℃ for 18 h. Fig. 1 shows the TEM and HRTEM images of a representative sample (TiO_2/g-C_3N_4(1.5)), which was demonstrated to have the best photocatalytic activity. From Fig.1 a and b we could see that TiO_2 nanoparticles were well dispersed on the surface of g-C_3N_4 with particle size less than 20 nm. The HRTEM image shows the characteristic lattice fringe of (001) and (101) facets (Fig. 1c), indicating the existence of exposed high energy (001) facet in the TiO_2 nanoparticles. The corresponding FFT pattern demonstrates that the TiO_2 is in the form of a single crystal and the angle between
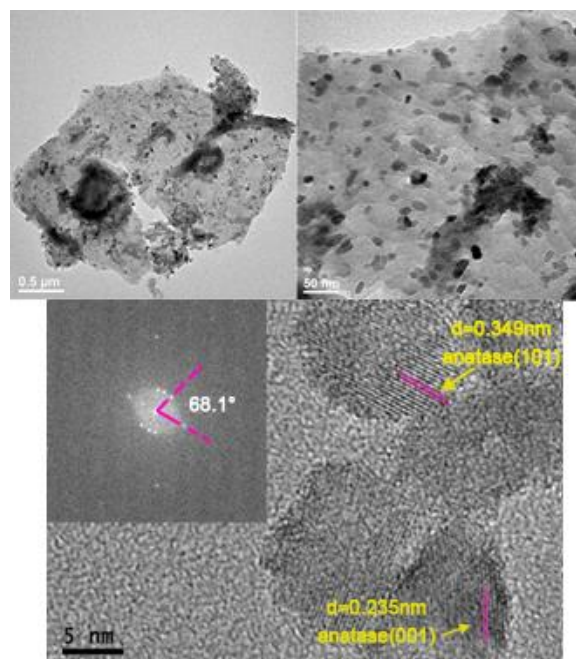
Fig.1 (a, b) TEM images for TiO_2 /g-C_3N_4(1.5); (c) HRTEM image for TiO_2 / g-C_3N_4(1.5), Inset is the corresponding fast Fourier transform (FFT) pattern.
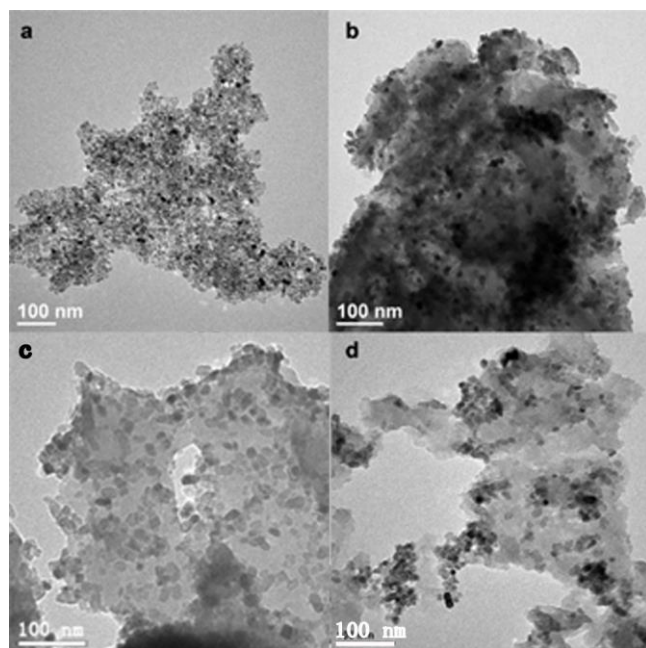
Fig.2 The TEM images of (a) TiO_2; (b) TiO_2/ g-C_3N_4 (0.5); (c) TiO_2/g-C_3N_4 (1.0); (d) TiO_2/g-C_3N_4(2.0).

(001) and the (101) plane is 68.1°, which is consistent with previous reports in terms of TiO_2 nanocrystals with (001) facet[43]. According to our previous study on the synthesis of TiO_2 nanomaterials[4], during the solvothermal process, AMAT can act as a catalyst for the hydrolysis of TBOT in the non-aqueous system. AMAT decomposes to produce acetic acid, which can esterify with ethanol to produce water molecules. These in situ produced water molecules catalyze the hydrolysis of TBOT, leading to TiO_2 nanoparticles with small particle size. However, if there is no g-C_3N_4 in the reaction system, the TiO_2 nanocrystals aggregate seriously as shown in Fig. 2a. And with the increase of g-C_3N_4 content in the reaction system (Fig. 2b-d), which means an increase in the ratio of g-C_3N_4 to TiO_2 in the composite, the dispersion degree of the TiO_2 nanoparticles can be enhanced gradually. Therefore, g-C_3N_4 plays a key role for the dispersion of the TiO_2 nanoparticles. This is mainly because the N in g-C_3N_4 can have electronic interactions with Ti[18,25], leading to the growth of the TiO_2 nanoparticles onto g-C_3N_4. Collectively, g-C_3N_4 and AMAT synergy achieve the highly dispersed growth of TiO_2 nanoparticles with small particle size. In addition, because carboxylic acid is easy to adsorb on the surface of anatase{001}, part of the acetic acid produced by the decomposition of AMAT is acting as face-growth inhibitors[44], slowing the growth of the (001) facet of TiO_2 in the TiO_2 nanoparticles, leading to the exposed high energy facts.

The crystal structure of the samples was determined by XRD, as shown in Fig. 3. Two pronounced peaks can be found in bare g-C_3N_4 at about 13.5 and 27.4°, which accord with the characteristic inter planar staking peaks of aromatic systems and the inter-layer structural packing, indexed as the (100) and (002) crystal planes for
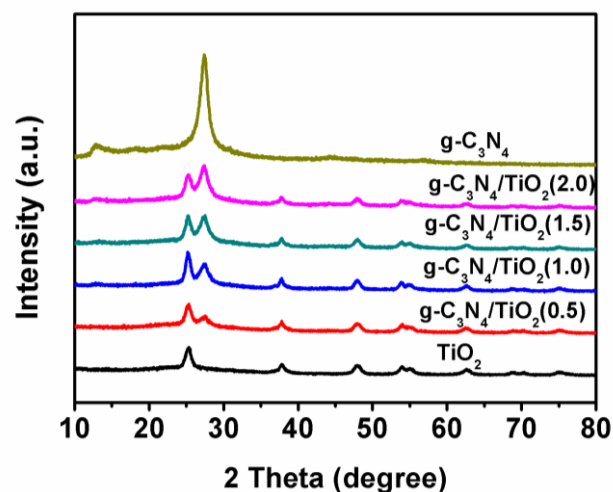
Fig.3 XRD patterns of the TiO_2 /g-C_3N_4 composites with different TiO_2 and g-C_3N_4 ratio.

graphitic materials, respectively[45]. The XRD pattern of bare TiO_2 which was prepared in the absence of g-C_3N_4 exhibits diffraction peaks with standard peak position and peak shape of anatase TiO_2 (JCPDF No. 21-1272)[46,47], which corresponds in turn from left to right to (101), (103), (004), (112), (200), (105), (211), (206) and (116) crystal planes of anatase TiO_2. It can be seen that the same anatase phase can be identified in the TiO_2/g-C_3N_4 nanocomposites with the bare TiO_2. As the content of g-C_3N_4 increased in the composited catalysts, the diffraction peak of g-C_3N_4 at about 27.4° gradually increases. Except for the peak at 27.4°, there are no obvious changes of the positions, intensities, and widths of characteristic diffraction peaks of anatase TiO_2. This fact suggests that the existence of g-C_3N_4 has no significant influence on the phase structure of the TiO_2 particles. In addition, the XRD peaks of this heterogeneous catalyst were composed by the superposition of characteristic peaks of g-C_3N_4 and TiO_2, which inferred that TiO_2 grew on the surface of g-C_3N_4 without any disturbing to the internal structure of g-C_3N_4.

The surface composition and chemical status of the elements in the prepared TiO_2/g-C_3N_4 sample were analysed by XPS. Fig. 4 and Fig.5 illustrates the XPS survey spectrum and high-resolution XPS spectra of different elements. The survey spectrum (Fig. 4) shows that the TiO_2/g-C_3N_4 surface is composed of C, N, O and Ti. From the XPS spectrum of C 1s shown in Fig. 5a, two peaks can be distinguished to be centred at 284.2 and 287.4 eV, respectively. The peak at 284.2 eV is exclusively assigned to the adventitious hydrocarbon from the XPS instrument. Another one at 287.4 eV is identified as carbon atoms that have one double and two single bonds with three N neighbours[48,49]. Fig. 5b is the high-resolution N 1s spectrum of the TiO_2/g-C_3N_4 (0.5). The asymmetrical feature of the observed N 1s peaks suggests the coexistence of distinguishable models. A signal deconvolution after Gaussian curve fitting is also displayed in Fig. 5b, pointing out chemically different N species in
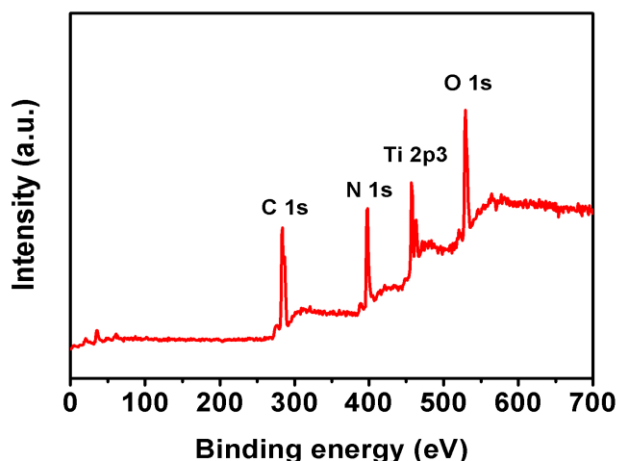
Fig.4 XPS survey spectra of TiO_2/g-C_3N_4(1.5).
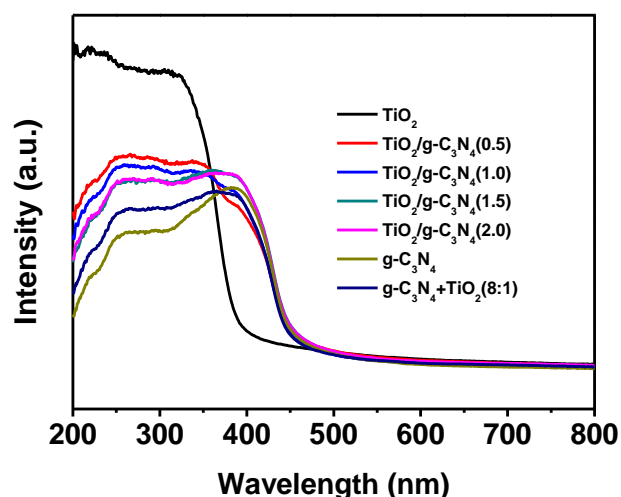
Fig.6 UV-Vis diffuse reflectance spectra (DRS) of different samples.
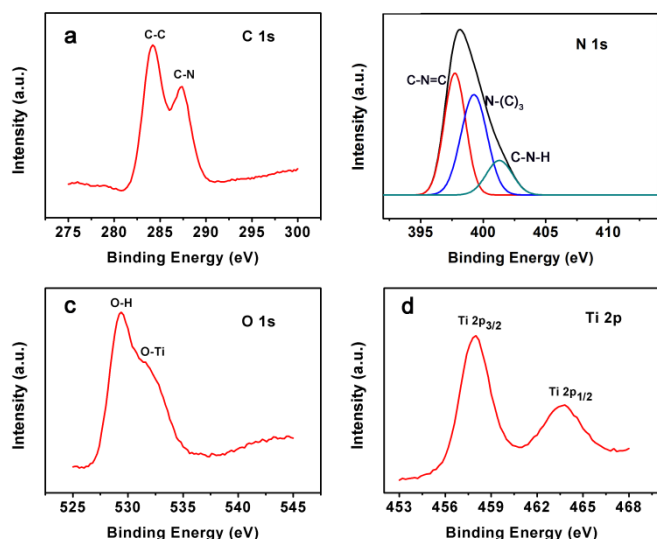
Fig.5 High-resolution XPS spectra of TiO_2/g-C_3N_4(1.5): (a) C 1s; (b) N 1s; (c) O 1s; (d) Ti 2p.

the g-C_3N_4, with their N 1s binding energy at 398.5, 399.6 and 400.8 eV, respectively. The N 1s binding energy of 398.5 eV can be assigned to sp2-hybridized nitrogen (C-N=C)[50]. The other two peaks at 399.6 and 400.8 eV can be attributed to tertiary nitrogen (N-(C)$_3$) and amino functional groups with a hydrogen atom (C-N-H), respectively[51]. The presence of the N-(C)$_3$ group confirm the polymerization of melamine[52]. From Fig. 3c and d, Ti 2p can be observed at binding energy of around 458.0 (Ti 2p$_{3/2}$) and 463.8 eV (Ti 2p$_{1/2}$)[53], while O 1s at binding energy of 529.4 and 531.6 eV, which are in good agreement with previous reports[54].

UV-vis diffuse reflectance spectroscopy (DRS) was carried out to investigate the optical properties of the TiO_2/g-C_3N_4 materials. Fig.6 is the results of UV-Vis diffuse reflectance spectra (DRS) of different

samples. From the spectra we could see that a sharp fundamental absorption edge for TiO_2 was 390 nm and the main absorption edge of the pure g-C_3N_4 occurs at 450 nm. The optical absorption of TiO_2/g-C_3N_4 is enhanced distinctly in both UV and visible light region compared to that of pure g-C_3N_4. This suggests that the growth of the TiO_2 on g-C_3N_4 can possibly cause modifications to g-C_3N_4 in the fundamental process of electron–hole pair formation during irradiation[58], which will be favorable for the photocatalytic reaction.

Photocatalytic activity and enhancement mechanism

The photocatalytic activity of the catalysts was evaluated by the photocatalytic degradation of phenol. It can be seen from Fig.7a that, after 90 min photocatalytic reaction, the degradation rate of phenol solution was 81% at the present of pure TiO_2. The degradation rate of phenol solution which was added pure g-C_3N_4 was only 70%. However, with the hybrid catalysts, the degradation all reached 100% within 90 min, suggesting the TiO_2/g-C_3N_4 composites exhibited higher photocatalytic activity than both the pure TiO_2 and pure g-C_3N_4 sample. From Fig. 7a we can also find that, with the content of g-C_3N_4 increase from 0.5 g to 1.5 g which means an increase of dispersion degree of TiO_2 nanocrystals on g-C_3N_4 as discussed above, the photocatalytic activity was enhanced gradually, proving the high dispersion of TiO_2 nanocrystals is beneficial for the enhancement of the photocatalytic activity. When the content of g-C_3N_4 reached 1.5 g, the as-prepared photocatalyst exhibited the highest photocatalytic activity. Significantly, the TiO_2/g-C_3N_4 (1.5) presents an obvious increase in the catalytic activity for phenol decomposition, which induced 100% degradation within 50 min. We can further describe and compare the photocatalytic properties of TiO_2/g-C_3N_4 (1.5) with pure g-C_3N_4 and pure TiO_2 by the photocatalytic degradation rate constants which was shown in Fig. 7b and determined by the first-order kinetic equation ln (C_0/C) = kt. Remarkably, the average value of rate
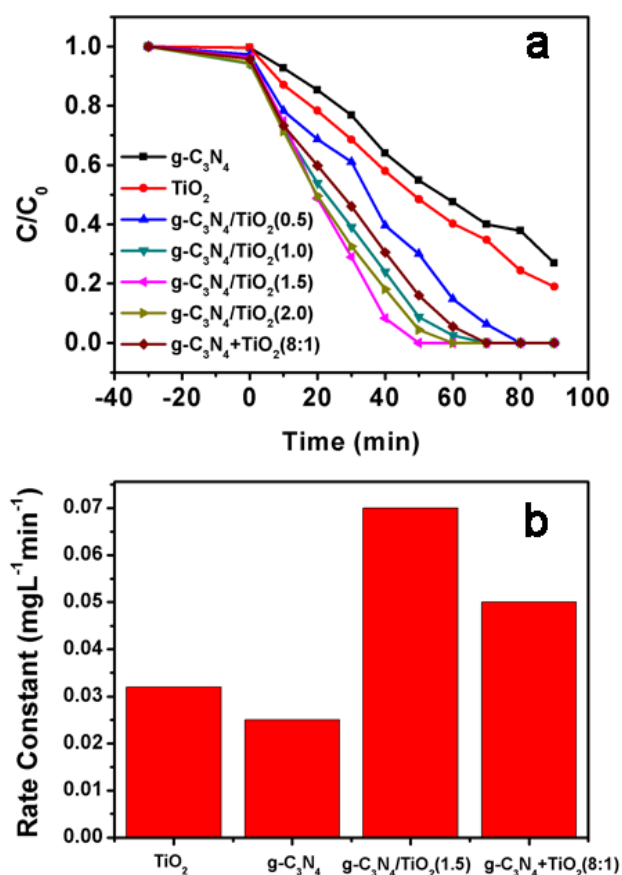
Fig.7 The photocatalytic degradation results to 10 mg/L phenol of different catalysts in the light source of 300 W Xenon lamp coupled with AM 1.5.

Fig.8 Thermal gravimetric (TG) analysis of TiO_2/g-C_3N_4 (1.5).

constant k of TiO_2/g-C_3N_4 (1.5) is about 2.2 times that of pure TiO_2 and 2.8 times that of pure g-C_3N_4. This result further demonstrates that the combination of TiO_2 and g-C_3N_4 can effectively improve the photocatalytic activity of both parts. However, further increasing the content of g-C_3N_4 in the composites to 2.0 g led to a decrease in the degradation rate of phenol under the same conditions. The reason to this phenomenon may be as following: If g-C_3N_4 increased longer, although the TiO_2 dispersed better on the g-C_3N_4, extra g-C_3N_4 would block the light exposing onto TiO_2. As a result, the catalytic activity reduced. Therefore, a suitable ratio of TiO_2 to g-C_3N_4 in the TiO_2/g-C_3N_4 composites was also necessary for achieving an optimum enhancement of the photocatalytic activity of g-C_3N_4. To verify whether the increased catalytic activity was associated with the interaction between g-C_3N_4 and TiO_2 or only a superposition of the activities of the two components, a control experiment using mechanically mixed g-C_3N_4 and TiO_2 for the photocatalytic degradation was performed. We adopted the method of thermogravimetric (TG) analysis to measure the mass ratio of g-C_3N_4 and TiO_2 in the TiO_2/g-C_3N_4 (1.5). Then we prepared the catalyst for the control experiment by mechanical mixing of g-C_3N_4 and TiO_2 in accordance with the ratio having been measured

by TG. Fig. 8 showed the TG results of heating TiO_2/g-C_3N_4 (1.5) from 40 ℃ to 880 ℃ in the air at the heating rate of 10 ℃/min. Because g-C_3N_4 became unstable when the temperature reached 600 ℃ in the air, at 700 ℃, g-C_3N_4 sublimated off completely by converting into nitrogen and cyano fragments. When the temperature was raised from 40 ℃ to 880 ℃, the g-C_3N_4 had completely sublimed away, and the leaving matter all was TiO_2, so we got the ratio of g-C_3N_4 and TiO_2. As Fig.8 shows, the mass fraction of final remaining material to total quality in TiO_2/g-C_3N_4 (1.5) was 11.2 %, that was to say the content of TiO_2 in TiO_2/g-C_3N_4 was 11.2 % and the quality ratio of g-C_3N_4 and TiO_2 was about 8:1. Therefore, we prepared the sample by mechanical grinding according to the ratio and labelled it as g-C_3N_4+TiO_2 (8:1). The photocatalytic result was also presented in Fig. 7. From Fig. 7a we can see that the phenol was degraded completely in 70 min, which is better than the pure g-C_3N_4 or pure TiO_2 but weaker than the in-situ prepared TiO_2/g-C_3N_4 (1.5). And the degradation constant rate of TiO_2/g-C_3N_4(1.5) is about 1.4 times that of g-C_3N_4+TiO_2 (8:1) (Fig. 7b) , indicating the in situ method is favourable for the enhancement of photocatalytic activity, which results from the uniform and close contact between g-C_3N_4 and TiO_2 through the in situ growth.

To further investigate the mechanism for the enhancement of the photocatalytic activity by growing TiO_2 nanocrystals on g-C_3N_4, photoluminescence (PL) spectra were measured. Fig. 9a was the results of PL spectra of pure g-C_3N_4, TiO_2/g-C_3N_4 (1.5) and g-C_3N_4+TiO_2 (8:1) under the excitation wavelength of 365 nm. PL emission measurement has been widely used to investigate the fate of electron-hole pairs in semiconductor particles because PL emission is known to result from the recombination of excited electrons and holes for some semiconductors[49,55]. The higher the PL emission intensity is, the higher the recombination efficiency of the photogenerated carriers is. As evident in Fig.9, the g-C_3N_4 sample exhibits strong photoluminescence at room temperature centered

ARTICLE
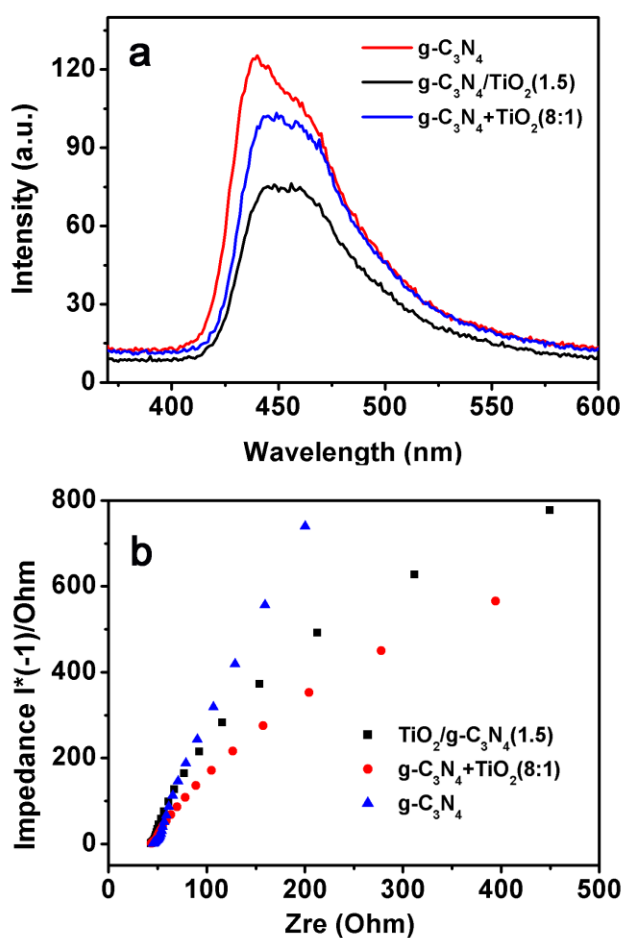
Fig.9 Photoluminescence spectra (a) and electrochemical impedance spectroscopy (b) of g-C_3N_4, TiO_2/g-C_3N_4 and g-C_3N_4+TiO_2(8:1).

at 450 nm. In comparison, the intensity of this emission band drops significantly for TiO_2/g-C_3N_4 (1.5). This indicates the growth of TiO_2 nanocrystals on g-C_3N_4 can inhibit the annihilation of the photogenerated electron–hole pairs and improve their separation efficiency. In addition, the TiO_2/g-C_3N_4 (1.5) sample has lower PL intensity than g-C_3N_4+TiO_2 (8:1), implying the in situ growth method can promote the charge separation more effectively, which is consistent with the photocatalytic activity of the samples. The electrochemical impedance spectroscopy (EIS) measurement reveals an analogous trend with respect to the PL spectra and photocatalytic activity. As can be seen from Fig. 9b, the EIS result reflects that the impedance arc radius of TiO_2/g-C_3N_4(1.5) is smaller than that of pure g-C_3N_4 and g-C_3N_4+TiO_2 (8:1) under simulated sunlight irradiation, indicating that TiO_2/g-C_3N_4 composite demonstrates enhanced separation efficiency of the photo-excited charge carriers compared with that of pure g-C_3N_4 and g-C_3N_4+TiO_2 (8:1)[56,57].

On the basis of the above experimental results, we believe that the enhanced photocatalytic activity induced by the in situ growth
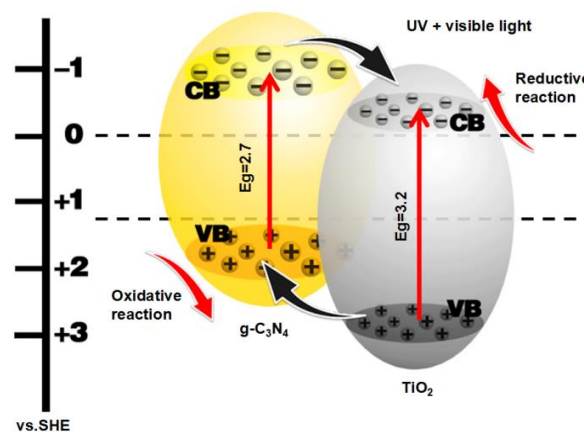
Fig.10 The transfer path mechanism of electrons and holes in the composited catalyst.

of TiO_2 is attributed to the effectively separation of photogenerated electron-hole pairs. Fig. 10 schematically shows the proposed mechanism for the promotion of the photocatalytic phenol degradation performance of TiO_2/g-C_3N_4. With the irradiation of simulated sunlight, both TiO_2 and g-C_3N_4 can absorb light to produce photo-induced electron-hole pairs. As the band positions of the g-C_3N_4 and TiO_2 match very well, the photogenerated electrons of g-C_3N_4 readily transfer to the conduction band (CB) of TiO_2, while the holes migrate from the valence band (VB) of TiO_2 to the VB of g-C_3N_4. In addition, the uniform and close contact between TiO_2 and g-C_3N_4 resulted from the in situ growth of highly dispersed TiO_2 nanocrystals promoted this interfacial transfer of photo-generated electrons and holes, as demonstrated by the photocatalytic result discussed above. Thus the recombination of photogenerated electrons and holes is sufficiently inhibited, leaving more electrons in the CB of TiO_2 and more holes in the VB of g-C_3N_4. Therefore, an effective charge separation can be achieved, resulting in longer lifetime of the photo-generated electrons and holes for enhanced photocatalytic activity. The photogenerated electrons in VB of TiO_2 could be used to catalyze a series of reduction reactions, and the photogenerated holes in CB of g-C_3N_4 could be used to catalyze series of oxidation reactions. All of these made the scope of application of this composite catalyst greatly broadened.

Conclusions

In this study, a simple solvothermal method has been developed for the in situ growth of TiO_2 nanocrystals on g-C_3N_4. The TiO_2 nanocrystals could achieve high dispersion on the surface of g-C_3N_4 and composed by only one nanocrystalline of anatase. In addition, there were some high energy (001) facets exposed. The photocatalytic activities of the composited catalysts were far greater than the pure catalysts (g-C_3N_4 or TiO_2) or the mechanically mixed catalyst, which was confirmed by the photocatalytic degradation experiments of phenol. The enhanced photocatalytic performance can be attributed to the increased charge separation in the composited catalysts derived from the well-constructed nano-architectures and well matched energy level between the TiO_2

and g-C$_3$N$_4$. This simple solvothermal method is quite hopeful to be extended for the synthesis of other semiconductor composited g-C$_3$N$_4$ in the applications of photocatalysis and other fields.

Acknowledgements

References

1   D. M. Schultz and T. P. Yoon, *Science*, 2014, 343, 1239176.
2   X. Guan, J. Du, X. Meng, Y. Sun, B. Sun and Q. Hu, *J. Hazard. Mater.*, 2012, 215, 1-16.
3   L. Lu, F. Teng, D. Qi, L. Wang and J. Zhang, *Appl. Catal. B: Environ.*, 2015, 163, 9-15.
4   D. Qi, L. Lu, Z. Xi, L. Wang and J. Zhang, *Appl. Catal. B: Environ.*, 2014, 160, 621-628.
5   P. Wang, J. Lei, M. Xing, L. Wang, Y. Liu and J. Zhang, *J. Environ. Chem. Eng.,* 2015, 592,1-8.
6   Y. Zhou, G. Chen, Y. Yu, Y. Feng, Y. Zheng, F. He and Z. Han, *Phys. Chem. Chem. Phys.*, 2015, 17, 1870-1876.
7   R. Sasikala, A. Gaikwad, V. Sudarsan, R. Rao, B. Viswanadh and S. Bharadwaj, *Phys. Chem. Chem. Phys.*, 2015, 17, 6896-6904.
8   J. Xu, C. Pan, T. Takata and K. Domen, *Chem. Commun*, 2015, 51, 7191-7194.
9   A. Reshak, *Phys. Chem. Chem. Phys*., 2014, 16, 10558-10565.
10   J. Liu, Y. Liu, N. Liu, Y. Han, X. Zhang, H. Huang, Y. Lifshitz, S.-T. Lee, J. Zhong and Z. Kang, *Science*, 2015, 347, 970-974.
11   Y. Zang, L. Li, X. Li, R. Lin and G. Li, *Chem. Eng. J.*, 2014, 246, 277-286.
12   Y. Zang, L. Li, Y. Zuo, H. Lin, G. Li and X. Guan, *RSC Adv.*, 2013, 3, 13646-13650.
13   S. Yan, Z. Li and Z. Zou, *Langmuir*, 2009, 25, 10397-10401.
14   X. Zou, Y. Dong, Z. Chen, D. Hu, X. Li and Y. Cui, *RSC Adv.*, 2015 (10.1039/C5RA01607J)
15   L. Huang, H. Xu, Y. Li, H. Li, X. Cheng, J. Xia, Y. Xu and G. Cai, *Dalton T.*, 2013, 42, 8606-8616.
16   X. Lü, J. Shen, D. Fan, J. Wang, Z. Cui and J. Xie, *Res. Chem. Intermediat.*, 2014, 40, 1911-1922.
17   J.-X. Sun, Y.-P. Yuan, L.-G. Qiu, X. Jiang, A.-J. Xie, Y.-H. Shen and J.-F. Zhu, *Dalton T.*, 2012, 41, 6756-6763.
18   J. Zhou, M. Zhang and Y. Zhu, *Phys. Chem. Chem. Phys.*, 2015, 17, 3647-3652.
19   J. Yu, S. Wang, J. Low and W. Xiao, *Phys. Chem. Chem. Phys.*, 2013, 15, 16883-16890.
20   J. Lei, Y. Chen, L. Wang, Y. Liu and J. Zhang, *J. Mater. Sci.*, 2015, 50, 3467-3476.
21   J. Lei, Y. Chen, F. Shen, L. Wang, Y. Liu and J. Zhang, *J. Alloy. Compd.*, 2015, 631,328-334.
22   S. Yan, S. Lv, Z. Li and Z. Zou, *Dalton T.*, 2010, 39, 1488-1491.
23   Y. Wang, Z. Wang, S. Muhammad and J. He, *CrystEngComm*, 2012, 14, 5065-5070.
24   C. Pan, J. Xu, Y. Wang, D. Li and Y. Zhu, *Adv. Funct. Mater.*, 2012, 22, 1518-1524.
25   S. Zhang, D. Yang, D. Jing, H. Liu, L. Liu, Y. Jia, M. Gao, L. Guo and Z. Huo, *Nano Res*., 2014, 7, 1659-1669.
26   Y. D, L. H, Z. Z, S. S and Z. H, *Nanoscale*, 2013, 6, 2232-2242.
27   L. Zhang, D. Jing, X. She, H. Liu, D. Yang, Y. Lu, J. Li, Z. Zheng and L. Guo, *J. Mater. Chem. A*, 2014, 2, 2071-2078.
28   Y. D, L. H, Z. Z, Y. Y, Z. JC, W. ER, K. X and Z. H., *J Am Chem Soc*, 2009, 131, 17885-17893.
29   M. Fu, J. Pi, F. Dong, Q. Duan and H. Guo, *Int. J. Photoenergy*, 2013, 2013, 1-7(10.1155/2013/158496).
30   H. Yan and H. Yang, *J. Alloy. Compd.*, 2011, **509**, L26-L29.
31   L. Gu, J. Wang, Z. Zou and X. Han, *J. Hazard. Mater.*, 2014, 268, 216-223.
32   Y. Zang, L. Li, Y. Xu, Y. Zuo and G. Li, *J. Mater. Chem. A*, 2014, 2, 15774-15780.
33   J. Zhou, M. Zhang and Y. Zhu, *Phys. Chem. Chem. Phys.*, 2015,17,3647-3652.
34   X. Lu, Q. Wang and D. Cui, *J. Mater. Sci. Technol.*, 2010, 26, 925-930.
35   Z. Huang, Q. Sun, K. Lv, Z. Zhang, M. Li and B. Li, *Appl. Catal. B-Environ.*, 2015, 164, 420-427.
36   J. Shen, H. Yang, Q. Shen, Y. Feng and Q. Cai, *CrystEngComm*, 2014, 16, 1868-1872.
37   X.-X. Zou, G.-D. Li, Y.-N. Wang, J. Zhao, C. Yan, M.-Y. Guo, L. Li and J.-S. Chen, *Chem. Commun.*, 2011, 47, 1066-1068.
38   H. Zhu, D. Chen, D. Yue, Z. Wang and H. Ding, *J. Nano. Res.*, 2014, 16, 1-10.
39   M. Fu, J. Liao, F. Dong, H. Li and H. Liu, *J. Nanomater.*, 2014,(10.1155/2014/869094).
40   Y. Li, J. Wang, Y. Yang, Y. Zhang, D. He, Q. An and G. Cao, *J. Hazard. Mater.*, 2015, 292, 79-89.
41   C. Hu, T. Lu, F. Chen and R. Zhang, *J. Chin. Adv. Mater. Soc.*, 2013, 1, 21-39.
42   H. G. Yang, C. H. Sun, S. Z. Qiao, J. Zou, G. Liu, S. C. Smith, H. M. Cheng and G. Q. Lu, *Nature*, 2008, 453, 638-641.
43   B. Qiu, M. Xing and J. Zhang, *J. Am. Chem. Soc.*, 2014, 136, 5852-5855.
44   R. Tanner, Y. Liang and E. Altman, *Surf. Sci.*, 2002, 506, 251-271.
45   G. Liao, S. Chen, X. Quan, H. Yu and H. Zhao, *J. Mater. Chem.*, 2012, 22, 2721-2726.
46   K. J. Lee, M. S. Maqbool, P. A. Kumar, K. H. Song and H. P. Ha, *Res. Chem. Intermediat.*, 2013, 39, 3265-3277.
47   F. Deng, X. Luo, H. Shu, X. Tu and S. Luo, *Res. Chem. Intermediat.*, 2013, 39, 2857-2865.
48   M. Ou, Q. Zhong and S. Zhang, *J. Sol-Gel Sci. Technol.*, 2014, 72, 443-454.
49   C. Miranda, H. Mansilla, J. Yáñez, S. Obregón and G. Colón, *J. Photochem. Photobiol. A: Chem.*, 2013, 253, 16-21.
50   L. Ye, J. Liu, Z. Jiang, T. Peng and L. Zan, *Appl. Catal. B: Environ.*, 2013, 142, 1-7.
51   H. Ji, F. Chang, X. Hu, W. Qin and J. Shen, *Chem. Eng. J.*, 2013, 218, 183-190.
52   Y. Sun, C. Li, Y. Xu, H. Bai, Z. Yao and G. Shi, *Chemi. Commun.*, 2010, 46, 4740-4742.
53   L. Zhao, M. Han and J. Lian, *Thin Solid Films*, 2008, 516, 3394-3398.
54   S.-X. Liu, X.-S. Li, X. Zhu, T.-L. Zhao, J.-L. Liu and A.-M. Zhu, *Plasma Chem. Plasma P.*, 2013, 33, 827-838.
55   R. Velmurugan and M. Swaminathan, *Res. Chem. Intermediat.*, 2015, 41, 1227-1241.
56   C. Zeng, M. Guo, B. Tian and J. Zhang, *Chem. Phys. Lett.*, 2013, 575, 81-85.
57   C. Zeng, B. Tian and J. Zhang, *J. Colloid Interface sci.*, 2013, 405, 17-21.

Table of Contents
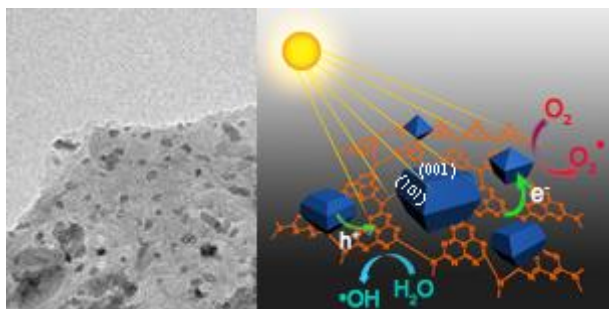
Highly dispersed TiO_2 nanocrystals with (001) facet were successfully grown in-situ on g-C_3N_4 through a facial method. The resultant composite exhibits remarkably enhanced photocatalysis comparing to pure TiO_2 or g-C_3N_4 or mechanically mixed TiO_2/g-C_3N_4.